CLM-P640

UKAEA

Preprint

THE SENSITIVITY OF TOKAMAK IGNITION CONDITIONS TO THE TRANSPORT MODEL AND IMPURITY RADIATION

I. L. ROBERTSON
J. G. CORDEY
J. J. FIELD

CULHAM LABORATORY
Abingdon Oxfordshire

1981

CLM-P640

THE SENSITIVITY OF TOKAMAK IGNITION CONDITIONS TO THE TRANSPORT MODEL AND IMPURITY RADIATION

I L Robertson, J G Cordey and J J Field
Culham Laboratory, Abingdon, Oxon, OX14 3DB, UK
(Euratom/UKAEA Fusion Association)

ABSTRACT

The sensitivity to the transport model of the plasma β at ignition and the additional heating power needed to reach ignition are calculated using a steady state 1-D transport code. Three empirical transport models with differing temperature behaviour are used and although the additional heating power is found to be strongly dependent upon the transport model, the β at ignition is found to be only weakly dependent upon the model.

Impurity radiation is found to mainly change the temperature profile and only has a small effect on the plasma β. The profile changes mean that a larger concentration of impurities can be tolerated at ignition than given by previous fixed profile calculations.

(Submitted for publication in Nuclear Fusion)

April 1981
cms

1 INTRODUCTION

To attain ignition in a tokamak two main conditions have to be satisfied. The first is that the plasma is MHD stable both on the approach to and during ignition, this places a restriction on the plasma β. The second is that sufficient heating power is available so that the ignited state can be reached. These both depend crucially on the transport properties of the plasma and the impurities, which are not sufficiently well understood for any precise calculation of the ignition parameters to be made. Nevertheless, several theoretical and empirical scaling laws have been proposed and in this paper we extrapolate these to the reactor regime. Not surprisingly we find that different scaling laws give rise to differing power requirements for ignition and critical β's at ignition. However the range of β values at ignition is quite narrow of the order of 5-8% for the JET parameters whereas the power requirements vary enormously (8-24 MW for pure plasmas). Interestingly increasing the concentration of impurities also results in a much larger change in the power needed for ignition than in the average β at ignition, which is not significantly affected by impurity radiation. This is because the main effect of impurity radiation is to alter the shape of the electron temperature profile, which becomes flatter in the outer region and more peaked in the centre.

Three different empirical scalings of the thermal conductivity that we consider are first the simple scaling used in the INTOR studies[1]

$$\chi_e = 5 \times 10^{19}/n \quad (m^2\ s^{-1}) \qquad (1.1)$$

second the form proposed by Coppi and Mazzucato[2]

$$\chi_e = 6.4 \times 10^{19} a\, Z_{eff}^{3/5} B_\phi/(nRq\, T_e) \qquad (1.2)$$

and the third form proposed by Ohkawa[3] and several other authors[4]

$$\chi_e = 1.4 \times 10^{20} T_e^{\frac{1}{2}}/nRq \qquad (1.3)$$

The above three forms have different temperature scalings and bracket the range of temperature behaviour seen in present devices. (All units in eq(1.1-1.3) are SI apart from T which is in keV.)

To determine the ignition curve and the optimum route to ignition for a particular model of the thermal transport a steady state 1-D transport code was used. The main advantage of such a code is that the thermally unstable low temperature side of the ignition curve can be readily determined. Since both the alpha particle heating and the impurity radiation are strong functions of temperature an adaptive non-uniform spatial grid technique is used so that reasonable numerical accuracy is achieved with an economy of grid points.

The structure of the paper is as follows. In section 2 the basic steady state transport equations are given, together with a brief description of the algorithm which is used for their solution.

Section 3 contains a discussion of the numerical results. First the ignition curves for a pure plasma are given for the three scaling laws. Then the effect of impurities on the temperature profiles and the ignition curves is discussed and this is followed by a calculation of the power requirements of the different scaling laws.

2 THE PLASMA TRANSPORT MODEL AND NUMERICAL ALGORITHM

The problem we are concerned with is the steady state solution of the plasma transport equations. We are principally interested in the electron and ion power balance equations,

$$\frac{1}{r}\frac{d}{dr}\left[r\left(n\chi_e\frac{dT_e}{dr} + \frac{3}{2}T_e D\frac{dn}{dr}\right)\right] + E_z J_z + P_e - \frac{3m_e}{m_i}\frac{nk}{\tau_e}(T_e - T_i) - S^e_{br} + S^e_\alpha = 0 \tag{2.1}$$

$$\frac{1}{r}\frac{d}{dr}\left[r\left(n\chi_i\frac{dT_i}{dr} + \frac{3}{2}T_i D\frac{dn}{dr}\right)\right] + P_i + \frac{3m_e}{m_i}\frac{nk}{\tau_e}(T_e - T_i) + S^i_\alpha = 0 \tag{2.2}$$

where the forms for electron thermal conductivity χ are given in eqs(1.1-1.3) and the forms assumed for the remainder of the terms are listed below.

First, in the electron power balance eq(2.1) for the convective loss we take the same diffusion coefficient as in the Intor studies[1], i.e.

$$D = 0.25\ \chi_e \tag{2.3}$$

In the thermonuclear regime the ohmic contribution to the power balance is negligible, but we include it for completeness,

$$E_z J_z = \eta_{||} J_z^2 \tag{2.4}$$

For the neoclassical parallel resistivity $\eta_{||}$ we take the recent expression of Hirshman et al[5].

For bremsstrahlung we use the expression of Glasstone and Lovberg[6]

$$S_{br}^{e} = 4.8 \times 10^{-37} Z_{eff}\, n^2 T_e^{\frac{1}{2}}\ Wm^{-3} \qquad (2.5)$$

For the α particle heating of the electrons

$$S_{\alpha}^{e} = F_{\alpha} F_{\alpha e}\, n^2\ \varepsilon_T (1-\varepsilon_T) \langle\sigma v\rangle k E_{\alpha} \qquad (2.6)$$

with ε_T given by Field and Minardi[7], $\varepsilon_T = n_T/(n_T+n_D) = 0.5$, for $\langle\sigma v\rangle$ we take the Brunelli fit[8], $E_{\alpha} = 3.52 \times 10^3$ keV. Since we are studying the steady state we need not include the effects of a finite slowing down time on the heating. F_{α} is the fraction of trapped α particles, we take $F_{\alpha}=1$ everywhere.

For the ions we use the neoclassical expression for the thermal conductivity given by Duechs et al[9]

$$\chi_i = \frac{0.68}{1 + 0.36\nu_i^*} \cdot \frac{Z_{eff}}{\tau_i}\ \rho_{i\theta}^2 \left(\frac{r}{R_o}\right)^{\frac{1}{2}} + \frac{Z_{eff}}{\tau_i}\rho_i^2\ (1+1.6q^2) \qquad (2.7)$$

$\rho_{i\theta}$ and ρ_i are the ion gyroradii in the poloidal and toroidal fields respectively.

$$\nu_i^* = Z_{eff}\ R_o \frac{B_T}{B_\theta}\left(\frac{R_o\ m_i}{rkT_i}\right)^{\frac{1}{2}} \frac{1}{\tau_i} \qquad (2.8)$$

with the ion-ion collision time $\tau_i = 6.6 \times 10^{17}\ T_i^{3/2}/n\log\Lambda$, S_{α}^{i} is the α-particle heating to the ions

$$S_{\alpha}^{i} = F_{\alpha} f_{\alpha i}\ n^2 \varepsilon_T (1-\varepsilon_T)\ \langle\sigma v\rangle k E_{\alpha} \qquad (2.9)$$

The density profile can be calculated self-consistently, although for parametric studies it is convenient to take the form,

$$n(r) = n_o\left(1-\alpha \tanh^{\gamma}\left(\frac{r}{a}\right)\right) \qquad (2.10)$$

By varying the parameters α and γ the density profiles of present experiments could be easily simulated. For most of the runs the parameter α was set equal to 2, and although γ was varied in the range 3-5 it had little effect on the ignition curves.

Similarly we can calculate the current density, but since the ohmic heating is unimportant we assume an MHD stable current density profile to be frozen into the plasma. Thus we take the current profile to be

$$j(r) = j_o(1-r^2/a^2)^{\nu} \qquad (2.11)$$

and then $q_a/q_o = \nu+1$. The corresponding poloidal magnetic field is given by

$$B_\theta(r) = \frac{\mu_o I}{2\pi r}\left\{1-(1-r^2/a^2)^{\nu+1}\right\} \qquad (2.12)$$

where I is the total plasma current. We choose $q_o=1$, and q_a is given by the machine parameters, so ν is uniquely determined.

For the additional heating terms, P_i, P_e in eqs(2.1) and (2.2) we shall assume that neutral injection is used and then P_i and P_e have the form

$$P_e = SK_e\varepsilon_o, \quad P_i = S(1-K_e)\ \varepsilon_o \qquad (2.13)$$

where S is the source rate is the number of particles deposited per unit volume per sec, and for a pencil beam has the form[10]

$$S = \frac{I_o}{4\pi^2 rR\lambda\sin\theta}\left\{\exp\left[-\frac{1}{\sin\theta}\int_r^a \frac{dr}{\lambda}\right] + \exp\left[-\frac{1}{\sin\theta}\int_{-r}^a \frac{dr}{\lambda}\right]\right\} \qquad (2.14)$$

and K_e is the fraction of the fast ion energy going to the electrons.

For the impurities the coronal equilibrium average ion model developed by Post et al[11] is used. The impurity density profile will be taken proportional to the plasma density that is the concentration of impurity $f = n_z/n$ is a constant across the profile. This is of course a very simple model but it has received considerable support from spectroscopic measurements on present experiments.

To solve the equations we non-dimensionalise them, by introducing suitable characteristic lengths and times and then reduce them to a set of first order ordinary differential equations. The boundary conditions used, in the physical variables, are,

$$\left.\frac{dT_i}{dr}\right|_{r=0} = \left.\frac{dT_e}{dr}\right|_{r=0} = 0 \qquad (2.15)$$

and at r=a,

$$T_i = T_e = T_L \qquad (2.16)$$

where the limiter value T_L was usually taken as low as 10 eV to be well below the peak in the impurity radiation curves for oxygen and iron.

The differential equations are differenced using the trapezoidal rule and the resulting set of non-linear algebraic equations is solved by using the Newton-Raphson method. An adaptive method due to Lentini and Pereya[12] is used in which an error tolerance is specified and the algorithm solves the equations to this tolerance, introducing additional grid points in regions with large gradients automatically, this results in the formation of a non-uniform spatial grid.

The accuracy requested was usually 1% and to achieve this the code needed about 40 grid points. Roughly half of these were distributed in the end region between r/a = 0.8 and 1. The strong variation of the radiation as a function of electron temperature at low values of T_e was the reason for the heavy concentration of points in the edge region.

3 RESULTS

A typical solution of eqs (2.1 - 2.2) is given in Fig.1 where the ion and electron radial temperature profiles are shown along with the radial power balance. It is clear from this particular case and inspection of other cases that in the ignition region the dominant terms in eqs(2.1 - 2.2) are the electron thermal loss, the alpha-particle heating, radiation and thermal equilibration terms. For the forms of χ_e given by eqs(1.1 - 1,3) we find, after putting the equations in non-dimensional form, that the peak temperatures are functions of $\bar{n}a$, f (the impurity concentration) and P (the total injection power) only. Thus although all of the terms used in the numerical calculation are for the JET parameter set (R=2.96 m, a=1.6m, B=3.4T, I=4.8 MA) the ignition curves etc. are given in terms of $\bar{n}a$, f, P, $\hat{T}_e$, $\hat{T}_i$ so that approximate results may be obtained for any device.

The ignition curve for the INTOR scaling law eq(1.1) and a pure plasma is shown in Fig.2. This 1-D ignition curve has the same basic shape as the 0-D ignition curves[13,14], it also has many similar properties. First at high electron temperatures, $\hat{T}_e$ above 15keV, the ion temperature is greater than the electron temperature. The reactor potential of this hot ion mode of operation ($T_i > T_e$) has been discussed previously by Cordey[15] and Clarke[16] using a 0-D treatment. It is found to be a common feature of all of the scaling laws of eqs(1.1 - 1.3), that at high temperatures and low densities $T_i > T_e$. The physical reason for this, is that at low densities and high electron temperatures, the electron-ion equipartition term is much smaller than the electron thermal transport and radiation terms, and so the electron and ions become uncoupled.

Another property that the 1-D and 0-D ignition curves have in common is their thermal stability. Kolesnichenko et al[17] have shown for the simpler case of $T_e = T_i = T$, and with different thermal transport, that provided the 1-D ignition curves are plotted in $\bar{n}a$, $\hat{T}$ space, the thermal stability properties are the same as those of the 0-D ignition curves. Namely that the left hand side of the ignition curve is thermally unstable, with a growth rate proportional to $\frac{\partial \bar{n}a}{\partial \hat{T}}$, and the right hand side is thermal stable. This theory can be trivially extended to include line radiation, the thermal transport of eqs(1.1-1.3), and unequal temperatures.

A more useful parameter than $\hat{T}_e$, from an MHD stability point of view, is the average plasma β defined as

$$\bar{\beta} = 2\mu_o \int_o^a (n(T_i+T_e) + P_\alpha) r dr \; / \; \int_o^a B_\phi^2 \, r dr \qquad (3.1)$$

where P_α is the α particle pressure.
Another definition of average β which is frequently quoted in stability analysis is the centrally weighted average β^*, defined as

$$\beta^* = 2\mu_o \left[\int_o^a n^2 (T_i + T_e)^2 r dr \right]^{\frac{1}{2}} / \int_o^a B_\phi^2 \, r dr \qquad (3.2)$$

In Fig.3 the ignition curves for the three different scalings are shown in $\bar{n}a$, β^* space. The minimum β^* for ignition ranges from 5% for the Coppi-Mazzucato[2] scaling to 8% for the more pessimistic temperature scaling given by eq(1.3).

We next look at the effect of impurity radiation on the ignition curves. For our impurity model ($n_z \propto n$) the bulk of the radiation is still from the low temperature edge region and the main consequence, as can be seen from Fig.4, is a flattening of the temperature profile in the outer region and an increased central

temperature to provide the extra alpha particle heating to sustain the additional radiative loss. The change in the ignition curve is shown in Fig.5. On the low temperature side of the ignition curve the increased radiation is accommodated by an increased central ion temperature $\hat{T}_i$, whereas on the high temperature side, $\hat{T}_i$ is reduced. This is simply because the peak of the α particle production rate lies between the low and high temperature portions of the ignition curve around 100 keV. The thermal stability properties of the ignition curve with impurities, i.e. unstable (stable) on the low (high) temperature side, of course remain the same, as mentioned earlier.

The change in the average parameters $\bar{\beta}$ and β^* with impurity concentration are given in Fig.6 for iron and Fig.7 for oxygen. For an iron impurity concentration of 0.25% (see Fig.6) we see that there is only a small increase in $\bar{\beta}$ ($\sim$ 20%) and β^* ($\sim$ 50%). This is an improvement over the fixed temperature profile calculations of Jensen et al[14] in which a concentration of 0.25% of iron leads to a doubling of the temperature and hence $\bar{\beta}$. For oxygen there is less change in the temperature profiles than for iron, because the majority of the radiation is bremmstrahlung, and so the increase in $\bar{\beta}$ with impurity concentration given in Fig.7, is similar to the fixed profile results[14]. The results in Figs.5-7 are for the INTOR transport model, eq(1.1), calculations for the other scalings also show that the general effect of impurities is to change the shape of the temperature profiles rather than the average temperature or β needed for ignition.

Turning now to the power needed to reach ignition. The additional heating is assumed to be neutral injection, and to simulate the conditions in JET as closely as possible, the fast neutrals are assumed to be 160 keV deuterons injected at right

angles to the field lines. The contours of constant power for the INTOR scaling are shown in plan view Fig.8(a) and isometric projection 8(b). The interesting point here is that there is an optimum route in $\bar{n}a$, β^* space to ignition. This 'ignition pass' is bounded on the high density side by radiation losses and on the low density side by electron thermal transport losses. The contour diagram has the same basic shape for all of the scaling laws, the only major difference is the power level required to get through the pass. These are compared in Fig.9, where the power to reach a particular ion temperature for a route through the ignition pass is given. As expected the favourable temperature behaviour of scaling law (1.2) (Coppi-Mazzucato) leads to a very low value of the minimum value of the power needed[14] for ignition ($\sim$ 8MW), whereas the unfavourable temperature scaling eq(1.3) gives significantly higher ($\sim$ 26 MW).

The uncertainty on the power requirements for ignition is compounded when one takes into account the uncertainty on the impurity concentration. This is shown in Fig.10 where the same path through the ignition pass is shown for various concentrations of oxygen and iron impurity, from which it can be seen that impurity concentrations of the order of 0.1% of iron and 2% oxygen, (which are typical of the present experiments) substantially increase the power that is needed to reach ignition.

4 CONCLUSION

The sensitivity of tokamak ignition conditions to the thermal transport model and the concentration of impurities has been investigated. The main conclusions are that the plasma β at ignition is fairly insensitive to the transport model and impurity radiation, provided the concentration of impurity is not greater than those of

present experiments, that is up to 0.25% of iron and 2% of oxygen. Increasing the impurity concentration leads to a marked change in the temperature profiles, flattening them in the outer region and increasing the central values, whilst the average temperatures, $\bar{\beta}$ and β^* are only slightly increased. These profile changes mean that greater impurity concentrations can be tolerated at ignition for a given average β than has been predicted by 0-D calculations.

It is found that there is an optimum heating route to ignition in $\bar{n}a$, T space, the 'ignition pass', on which the required additional heating power is a minimum. This minimum power level is however found to be both strongly dependent on the transport model and the concentration of impurities.

REFERENCES

[1] INTOR, Plasma Physics and Controlled Fusion Research, EUR FU BRU/XII 501/79/EDV80, IAEA Vienna (1979).

[2] Coppi B and Mazzucato E, Phys.Letts A 71A (1979) 337.

[3] Ohkawa T, Report GA-A14433, General Atomic Co, San Diego, California, USA (1977).

[4] Drake J F, Gladd N T, Liu C S and Chang C L, Phys.Rev.Letts 44 (1980) 994.

[5] Hirshman S P, Hawryluk R J and Birge B, Nuc.Fus. 17 (1977) 611.

[6] Glasstone S and Lovberg R H, 'Controlled Thermonuclear Reactors' Van Nostrand (1960).

[7] Field J J and Minardi E, Culham Laboratory Report, CLM-R191 (1978).

[8] Brunelli B, Frascati Report CNEN G178/11 (1978).

[9] Duechs D F, Post D E and Rutherford P H, Nuc.Fus. 17 (1977) 565.

[10] Cordey J G, "Physics of Plasmas Close to Thermonuclear Conditions", EUR FU BRU/XII/476/80, Varenna, Italy (1979) 359.

[11] Post D E, Jenson R V, Tartar C B, Grassberger W H and Lokke W A, Atomic Data and Nuclear Data Tables, 20 (1977) 397.

[12] Lentini M and Pereyra V, SIAM J.Numer.Anal. 14 (1977) 91.

[13] Kesner J and Conn R W, Nuc.Fus. 16 (1976) 397.

[14] Jenson R V, Post D E and Jassby D L, PPPL-1350 (1977): Meade D M, Nuc.Fus.14 (1974) 289.

[15] Cordey J G, "Theory of Magnetically Confined Plasmas" Varenna (1977) 307.

[16] Clarke J F, Nuc.Fus. 20 (1980) 563.

[17] Kolesnichenko Ya I, Reznik S N, Yavorskij V A, Nuc.Fus.16 (1976) 105.

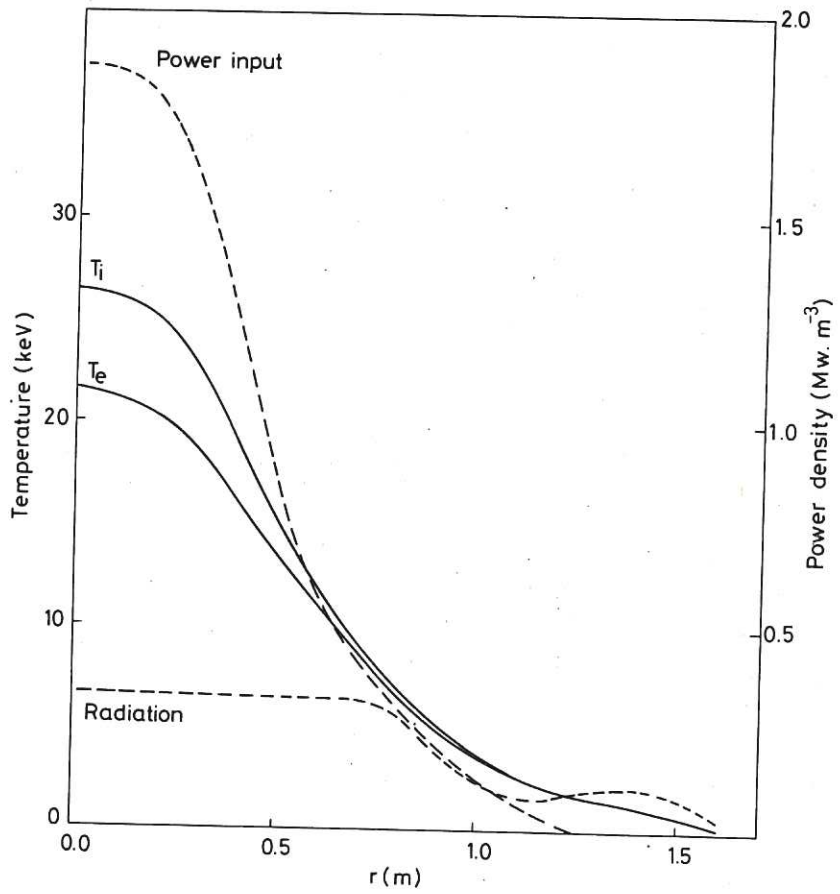

Fig.1 Electron and ion temperature profiles and radial power flow for a typical case.

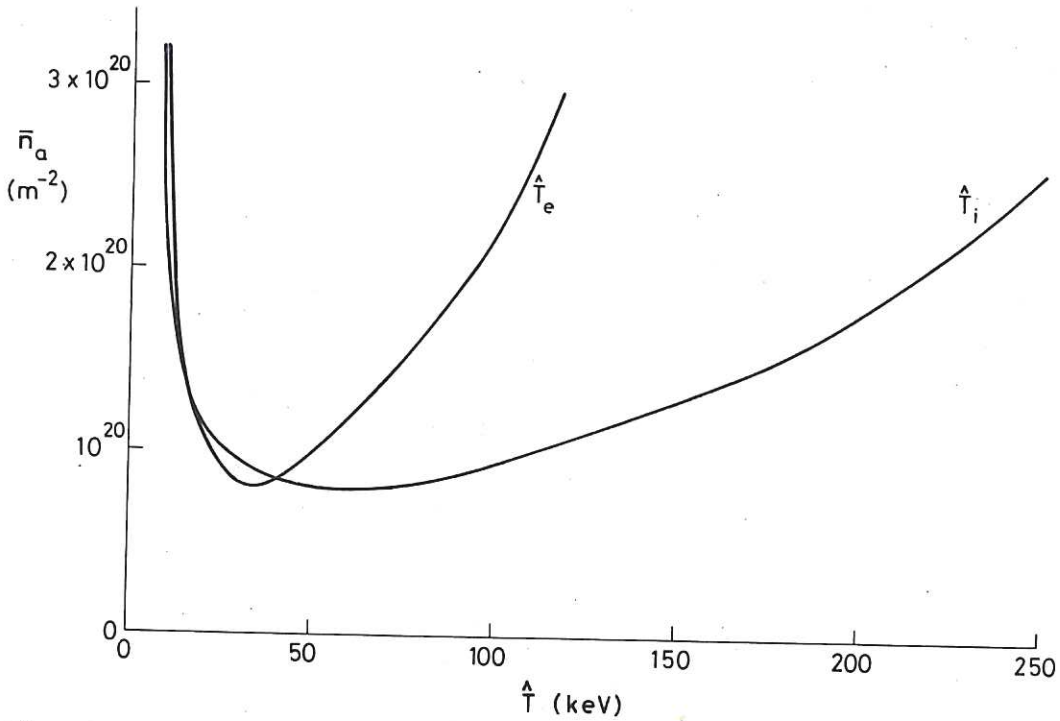

Fig.2 The ignition curve for a pure plasma and the INTOR scaling equation (1.1) in $\bar{n}a$, $\hat{T}_e$ space.

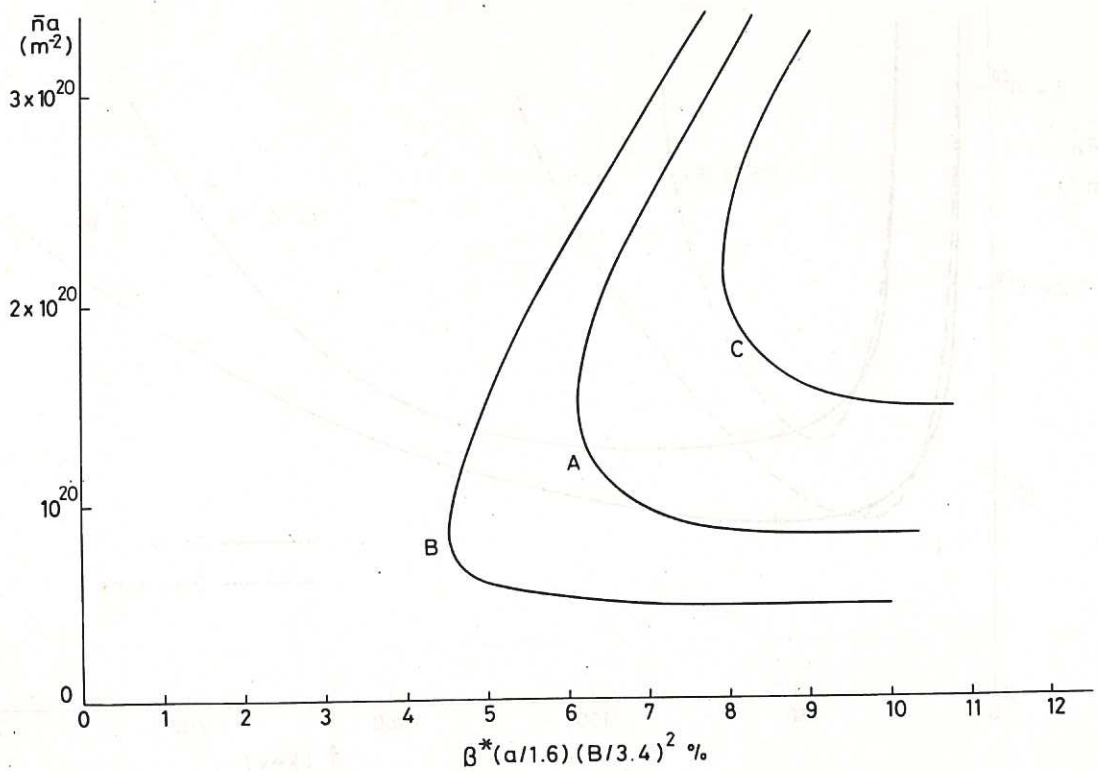

Fig.3 The ignition curves for the three scaling laws in $\bar{n}a$, β^* space (the factor $(a/1.6)(B/3.4)^2$ is included in β^* so that the results can be scaled to machines other than JET, a is the minor radius in metres, B is the toroidal field in tesla). Curve A is the INTOR scaling law eq.(1.1), curve B is the scaling suggested by Coppi and Mazzucato eq.(1.2) and C is the unfavourable temperature scaling law eq.(1.3).

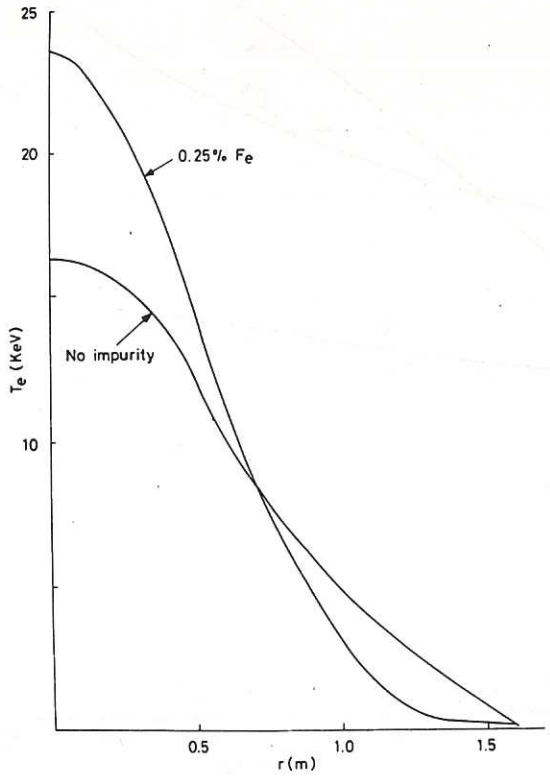

Fig.4 Comparison of the electron temperature profiles at ignition for an iron impurity concentration f of 0·25% and no impurity.

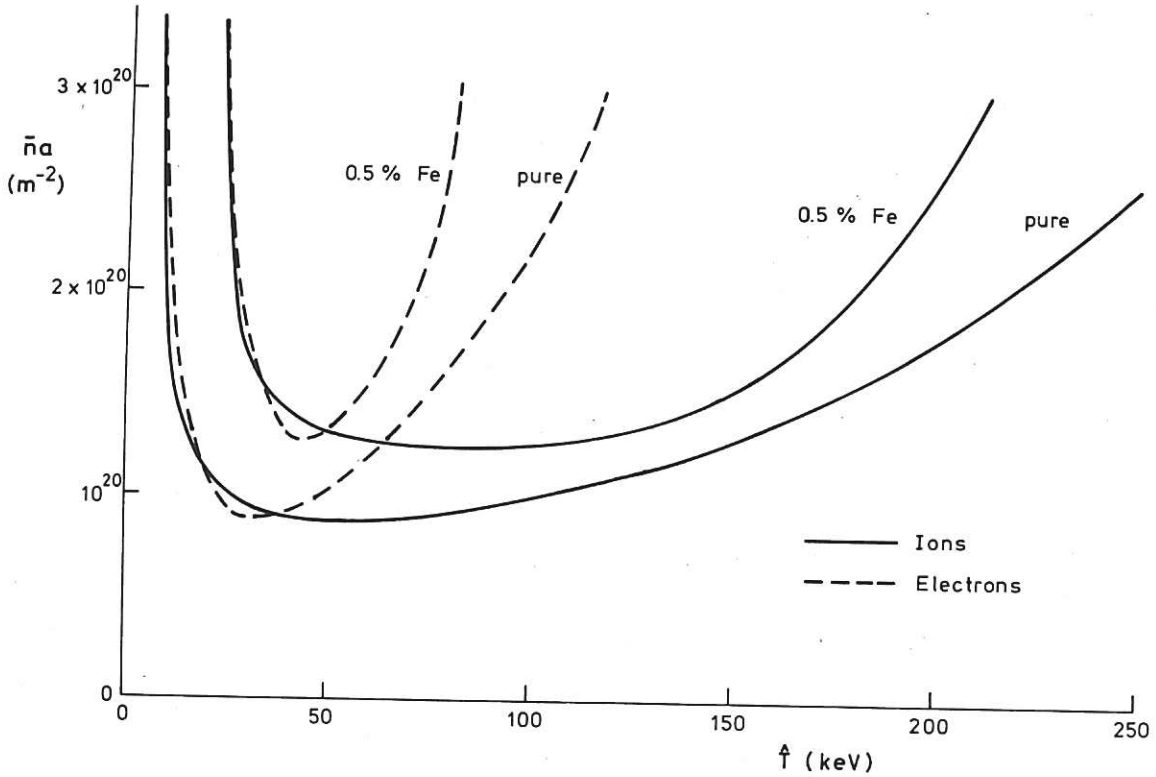

Fig.5 A comparison of the ignition curves in $\bar{n}a$, $\hat{T}$ space for a pure plasma and an impure plasma.

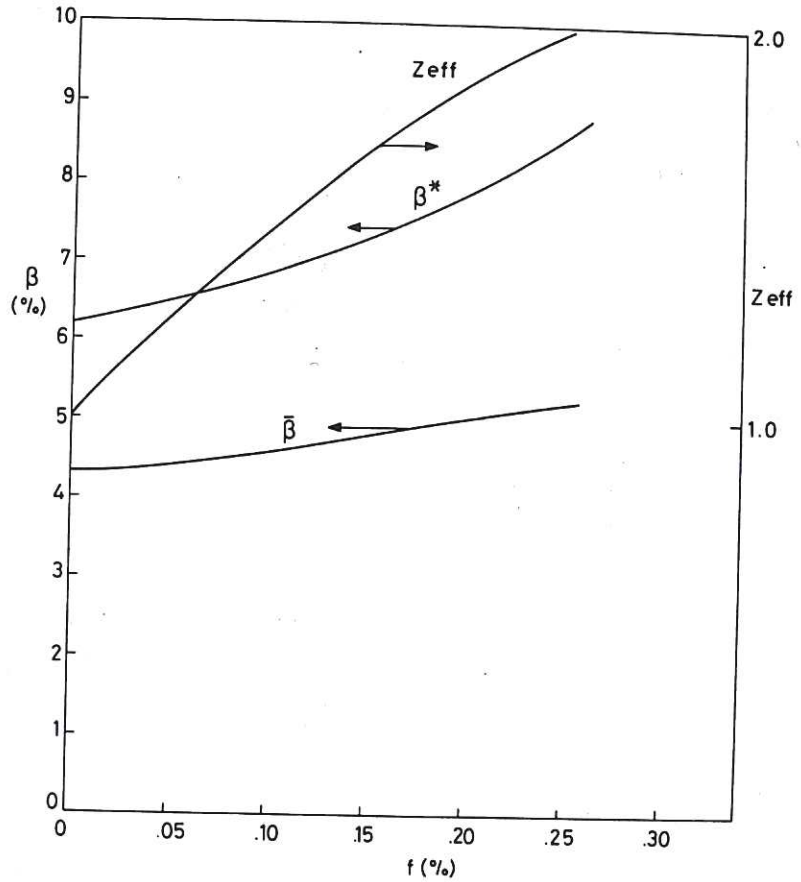

Fig.6 $\bar{\beta}$ and β^* at ignition versus f the concentration of iron impurity for INTOR scaling.

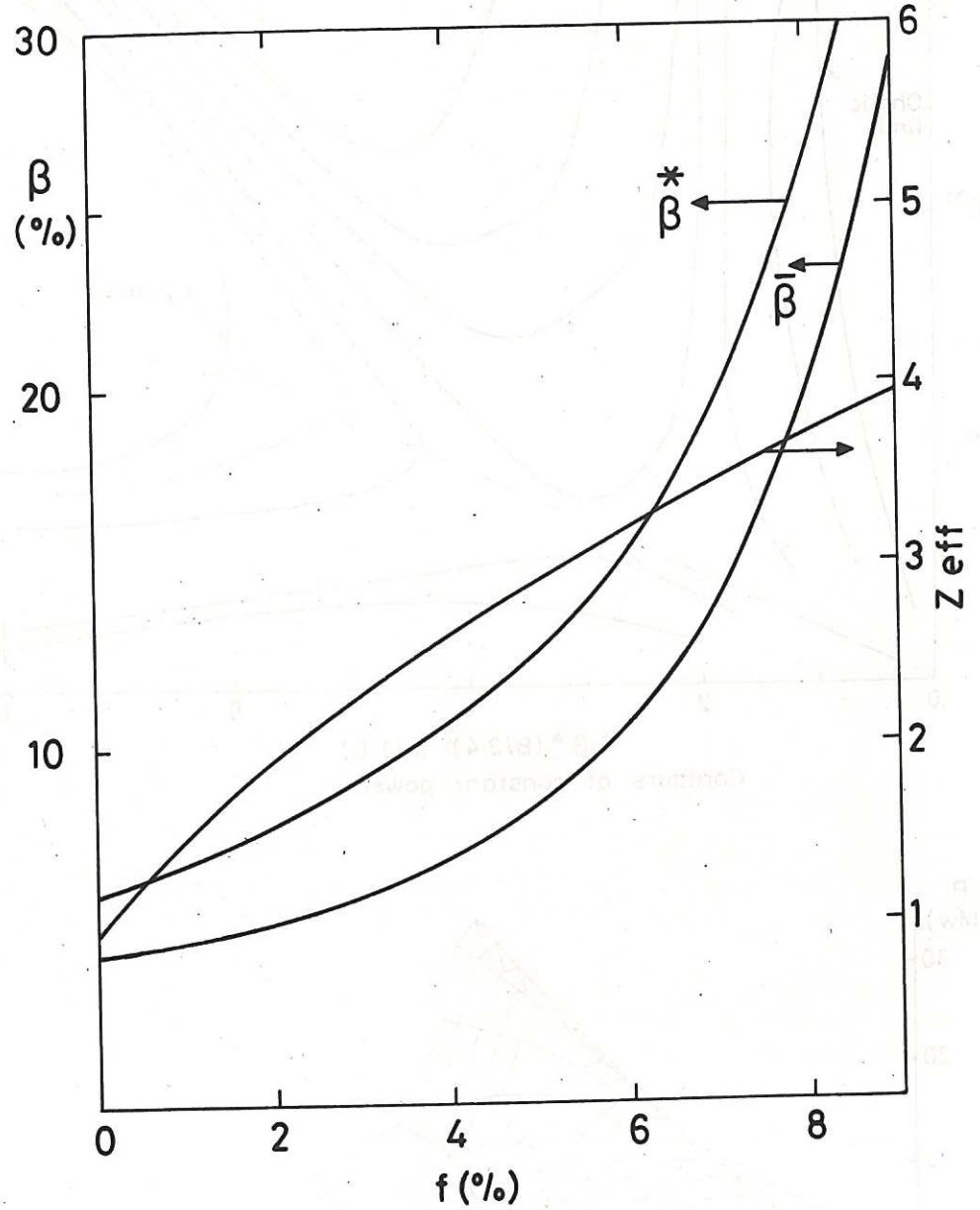

Fig.7 $\bar{\beta}$ **and** β^* **at ignition versus f the concentration of oxygen impurity for INTOR scaling.**

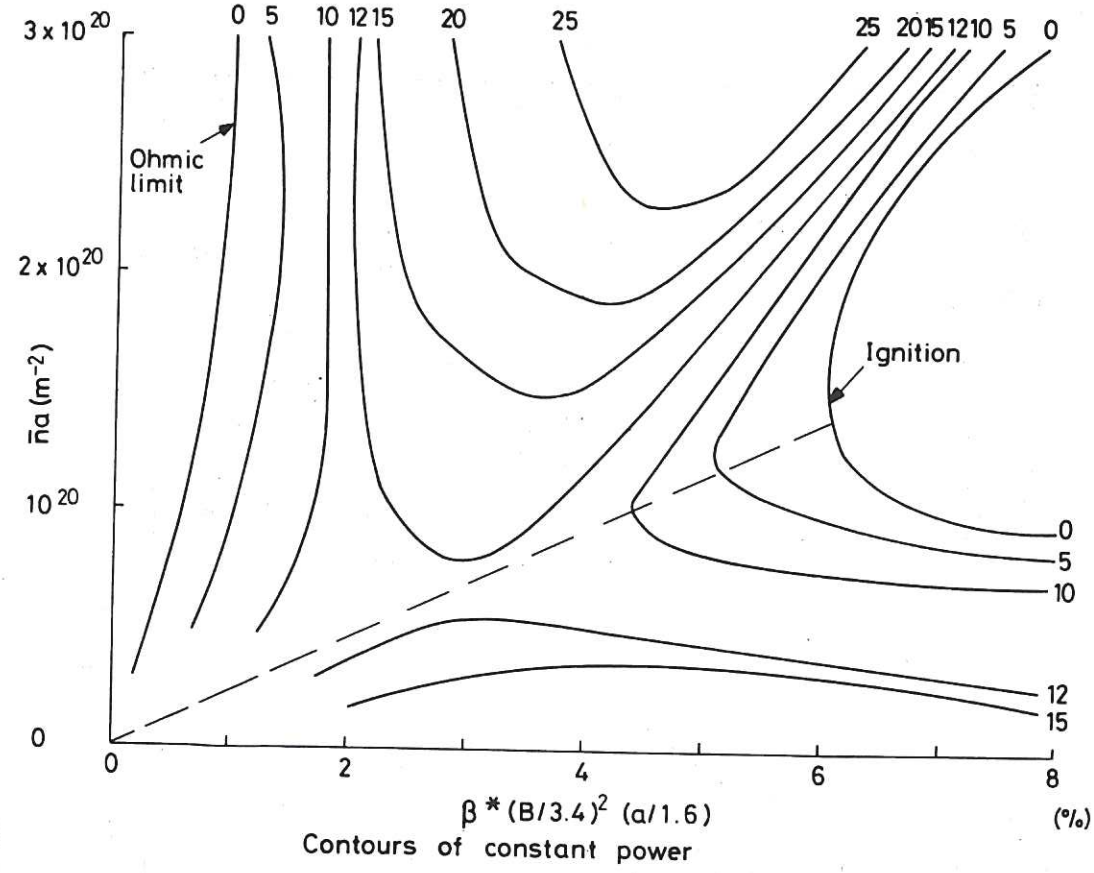

(a)

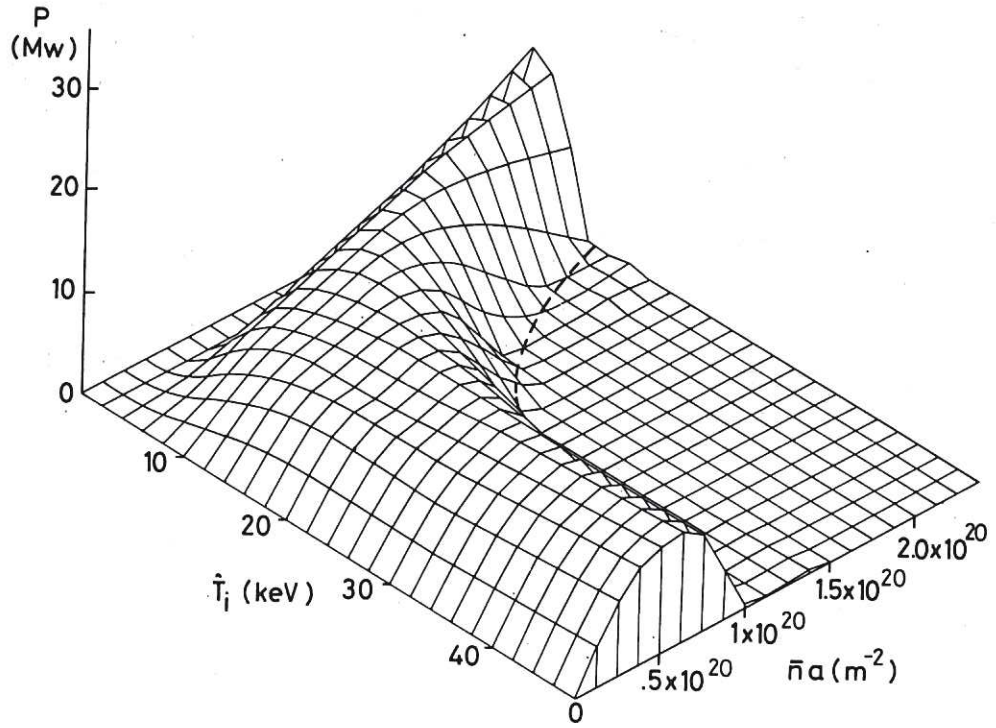

(b)

Fig.8 (a) Power contours in MW in $\bar{n}a$, β^* space; (b) Isometric projection of power versus $\bar{n}a$, $\hat{T}_i$.

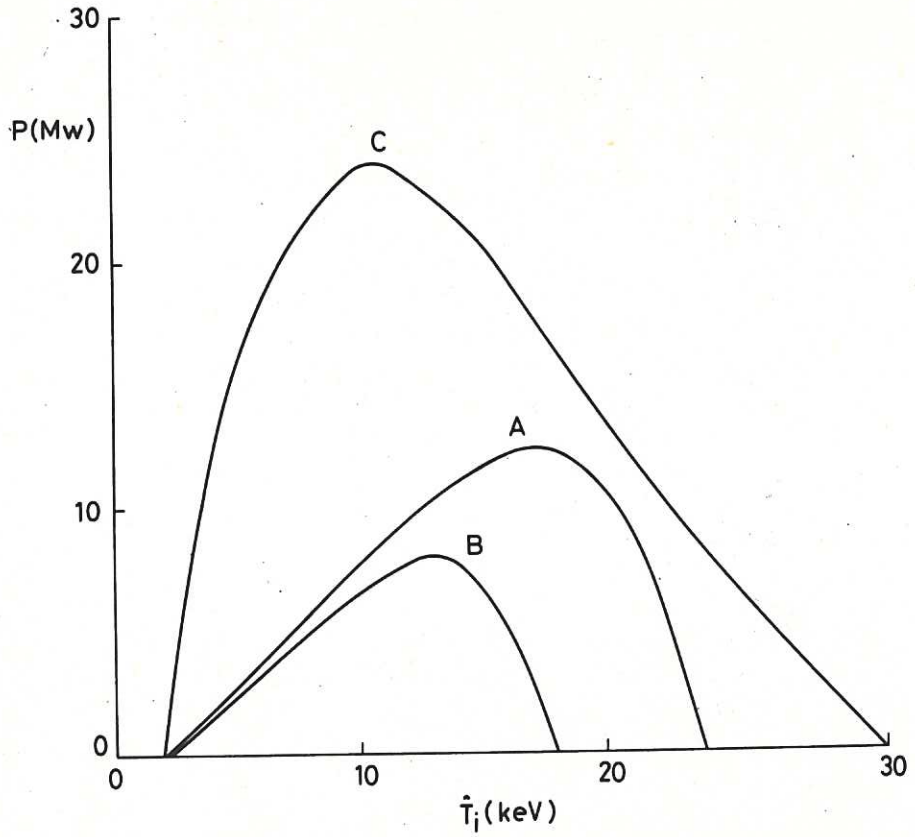

Fig.9 Injection power in MW versus $\hat{T}_i$ for the three thermal transport scalings, Curve A is eq.(1.1), B is eq.(1.2), C is eq.(1.3). The route to ignition is through the ignition pass.

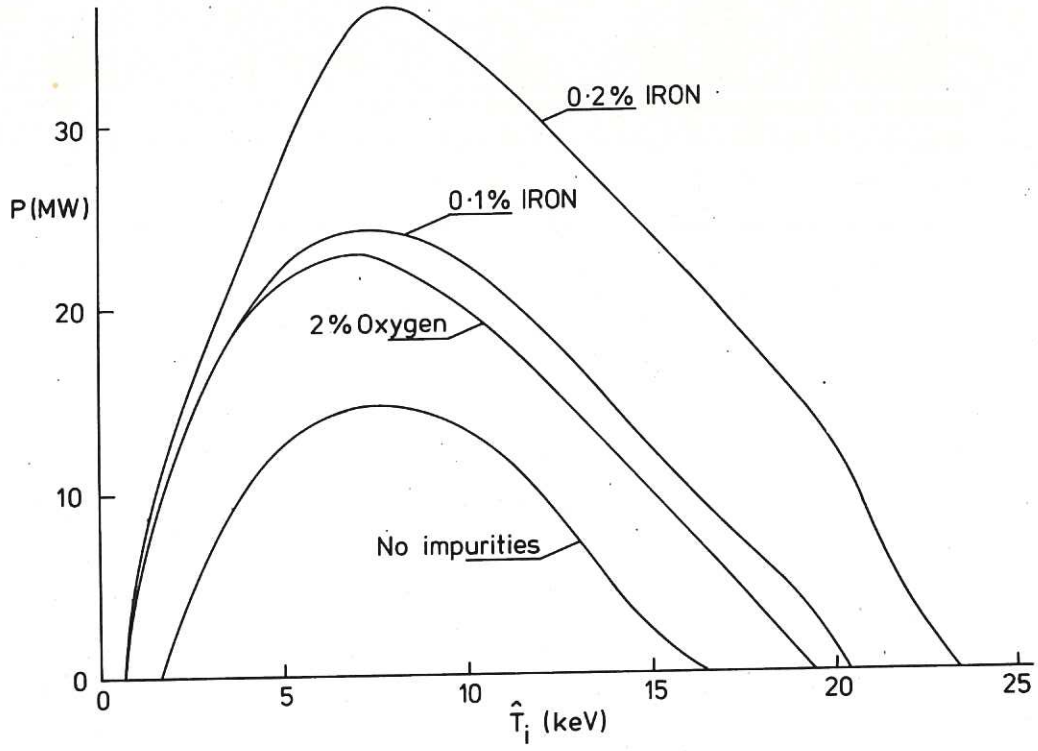

Fig.10 Injection power in MW versus $\hat{T}_i$ for different impurity concentrations on the route through the ignition pass. The thermal transport is INTOR.